CrystEngComm

COMMUNICATION

Supramolecular Assembly Through Intermolecular n → π* Interactions through a Coordinated Perrhenate Formed *via* Superoxidation of Re(I) to Re(VII) in the Formation of Substituted $Re(CO)_3$ Complexes Bearing Diimine Ligands

Received 00th January 20xx,
Accepted 00th January 20xx

DOI: 10.1039/x0xx00000x

www.rsc.org/

Reza Kia,*[a] Tahereh Taghavi[a] and Paul R. Raithby[b]

We report the structural, spectroscopic, and computational studies of two new Re(I) tricarbonyl complexes bearing 2,3,6,7-tetraphenyl-1,4,5,8-tetraazaphenanthrene (Ph_4TAP) and 4,5-diazafluoren-9-one (Dafone) having a coordinated perrhenate group obtained *via in situ* superoxidation of Re(I) to Re(VII); intramolecular and intermolecular n→π* interactions are dominant and stabilize the molecular geometry and crystal packing.

Noncovalent interactions are of key importance in numerous chemical and biological processes and in materials science.[1] Among the noncovalent interactions which are the basis of supramolecular chemistry, those involving lone pair···π-systems (lp···π) are of great importance in both chemistry and biology. The occurrence of such an interaction was reported first by Bürgi *et al*. in the structural study of (*S*)-methadone in which the nucleophilic dimethylamine segment moves close to the carbonyl group.[2] Following the observation of this significant structural feature, they proposed a geometrical reaction pathway for compounds containing nucleophilic and electrophilic centres; the reaction coordinates could be mapped along a minimum energy pathway, the so called Bürgi-Dunitz trajectory.[3] Since (lp···π) interactions have been proposed, most of the studies have focused on biomolecules and organic compounds.[4-20] The first systematic CSD and computational studies of carbonyl···carbonyl interactions in organic compounds and first-row transition metal complexes were reported by Allen, Raithby and *co-workers* in 1998 and 2006, respectively.[21] In 2011 and 2012, Zukerman-Schpector *et al*., highlighted the importance of the intermolecular metal-carbonyl···π(aryl) interactions as a supramolecular synthon for the stabilisation of transition metal carbonyl crystal structures.[22] Notably, although a survey of the Cambridge Structural Database (CSD) indicated that lp(O)···π* interaction occurs widely in organic and biomolecules, its role in the construction of supramolecular assemblies in metal complexes especially with M—CO···π*(aryl), M—CO···π*(C≡O) interactions, and peripheral carbonyl···π*(C≡O) (Scheme 1), remained unidentified until the first papers by Echeverría.[23-24] Additionally, Mooibroek *et al*. studied the potential of coordinated nitrate anions, acetonitrile, and carbonyl ligands as π-hole donors for n→π* in their crystal structures thorough analysis of the CSD.[25] It has been emphasised that intramolecular M—CO···π* interactions are prevalent in their structures and stabilise precise internal molecular conformations through maximizing the overlap between the donor and acceptor π*-orbitals involved in such interactions; This has been shown to make an important contribution in catalytic processes.[24, 26] These interactions can contribute significantly to the crystal packing and control supramolecular architectures despite the individual interactions being inherently weak. To this effect, the study of metal carbonyls complexes on the basis of participation in a n→π* interaction similar to their organic counterparts and related to their role in catalysis are of considerable interest. Therefore, in a continuation of our interest in intra- and intermolecular n→π* interactions in metal-carbonyl complexes, [27-30] herein, we report the synthesis, full structural and computational studies of two new $Re(CO)_3$ complexes bearing diimine ligands with a coordinated perrhenate, formed via superoxidation of Re(I), and its potential as supramolecular synthon for assembly through n→π* interactions.

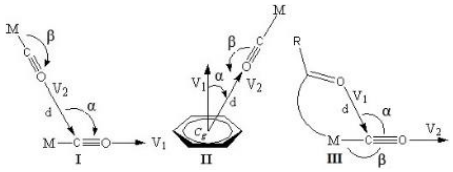

Scheme 1. Common geometry of the intermolecular lp(O)···π interaction in metal carbonyls. C_g is the centroid of the ring.

Complexes **1** and **2** were synthesized by the substitution reaction of $Re(CO)_5Br$ with *Ph_4TAP* and *Dafone* ligands (Scheme 2) through *cis* activation in refluxing toluene, in air. During the reaction perrhenate anions $[ReO_4]^-$ were formed by *in situ* oxidation of Re(I) to Re(VII) and these anions coordinated to

[a]*Chemistry Department, Sharif University of Technology, P.O. Box 11155-3516, Tehran, Iran. E-mail: rkia@sharif.edu, zsrkk@yahoo.com;* [b]*Department of Chemistry, University of Bath, Claverton Down, Bath, BA2 7AY, UK*

Electronic Supplementary Information (ESI) available: Experimental and computational details, FT-IR, ESI-MS, ^{1}H NMR, crystallographic data and structure refinement details, optimised Cartesian coordinates, NCI plots of the dimers.

the $[Re(CO)_3(Ph_4TAP)]^+$ and $[Re(CO)_3(Dafone)]^+$ cations to form the neutral di-rhenium mixed oxidation state complexes in good yields (69% for **1** and 70% for **2**). The presence of the *fac*-$[Re(CO)_3]^+$units in the two products was confirmed by IR spectroscopy. Complex **1** shows three bands related to carbonyl stretching at 2029, 1938 and 1901 cm^{-1} confirming C_s symmetry while complex **2** shows a sharp band at 2018 and a broad band at 1893 cm^{-1}, suggesting C_s spectroscopic symmetry (Fig. S1 & S2 in the ESI). The stretching mode of Re–O bond in **1** and **2** were observed at 842 cm^{-1}. The asymmetric and symmetric stretching modes of Re=O appeared at 920 and 1018 cm^{-1} for **1** and at 902 and 1108 cm^{-1} for **2**.[31] The ^1H NMR spectra (Fig. S3-S6) and the elemental analyses of **1** and **2** were consistent with the X-ray structures and confirmed **1** and **2** as the major reaction products (Fig. 1). Electrospray ionization (ESI) mass spectra (positive mode) showed a base peak at *m/z* 797.0439 and 481.0038 assignable to $[Re(CO)_3(Ph_4TAP) + K]^+$ and $[Re(Dafone)(CO)_4]^+$ in **1** and **2**, respectively which were confirmed by the simulated spectrum. The details of the experimental and simulated ESI-MS spectra for **1** and **2** are summarized in Fig. S7-S8. Single crystals of **1** and **2** were obtained by vapour diffusion of n-hexane into dichloromethane solution of the complexes. The crystal data, bond lengths and angles of **1** and **2** are summarized in Table S1 and 2. In each complex, the geometry around the Re(I) centre is distorted octahedral coordinated by the two iminic nitrogen atoms of *Ph₄TAP* in **1** and *Dafone* in **2**, three carbonyl groups in the *facial* arrangement, and the tetrahedral perrhenate group is coordinated through one of the peroxide oxygen atoms.

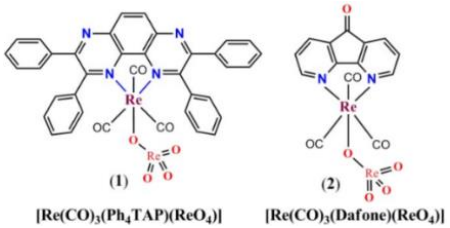

Scheme 2. Chemical scheme of complexes **1** and **2**.

The X-ray diffraction analysis revealed that the bite angle N1–Re1–N2 in **1** [76.72(7)°] is slightly more acute compared to that in **2** [78.5(2)°], consistent with shorter Re–N bonds in **1** [2.2053(19) & 2.2015(19) Å]. The equatorial metal-bound carbonyl groups show the intramolecular π(phenyl)···π*(C≡O) interactions with C2≡O2···*Cg1* and C3≡O3···*Cg2* distances of 3.010(2) and 3.016(2) Å, respectively, (Cg1 and Cg2 are the centroid of the C14-C19 and C26-C31 rings) in which the C2≡O2 [1.156(3) Å] distance is slightly longer than C3≡O3 [1.142(3) Å] in **1** at the 3σ significance level, consistent with a stronger interaction of C2≡O2 to the π-system (Fig. S9). The intramolecular C2···C14 and C3···C26 contacts are also shorter than sum of their van der Waals (vdW) radii (Fig. S9).[32] In each complex, the coordinated perrhenate is tilted towards the π-system of the diimine ligands due to the intramolecular n→π* interaction of lp(O5)···π*(N1=C7) and lp(O5)···π*(N2=C6) in **1** and lp(O8)···π*(N2=C9) in **2**. The interesting feature of the crystal packing of **1** is the intermolecular lp(O1)···π*(C4=C5) and lp(O6)···π*(C6=C7) interactions, due to the lone pair of the metal-bound carbonyl and perrhenate respectively which are shorter than sum of the vdW radii of the involved atoms. These interactions along with the intermolecular non-classic C–H···O hydrogen bonding link neighbouring molecules in a head-to-tail fashion generating an extended one-dimensional chain along the *b*-axis (Fig. 2 & Fig. S10). In **2** the equatorial carbonyl [C3≡O3 = 1.149(9) Å] is involved in two intermolecular n→π* interactions as lp(O1)···π*(C3≡O3) and lp(O8)···π*(C3≡O3), comparing to C1≡O1 which is involved only in one reciprocal antiparallel CO···CO interaction and there are no interaction for C2≡O2 (Fig. 3). The higher estimated standard deviations on the C≡O bond parameters in this structure compared to those in **1** precludes any detailed analysis of their bonding.

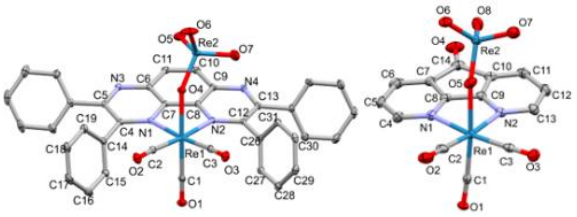

Figure 1. Molecular structure of **1** and **2** with 40% ellipsoids probability and selected atoms numbering. The H-atoms were omitted for clarity.

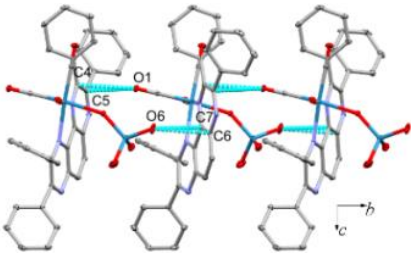

Figure 2. The crystal packing of **1** showing extended chain through intermolecular n→π* interactions (without H atoms).

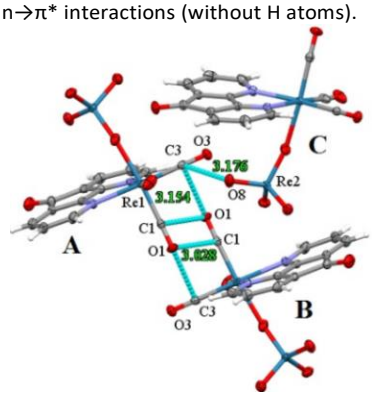

Figure 3. Representation of the intermolecular n→π* interactions involved in metal-bound carbonyl ligands [symmetry codes: (A) x, y, z; (B) 1-x, 1-y, 1-z (C) 1-x, -½+y, ½-z].

The interesting feature of the crystal packing of **2** is the presence of several different intermolecular n→π* interactions such as lp(O6)···π*(C8=C9), lp(O7)···π*(C10=C14), and lp(O7)···π*(C14=O4) which connect neighbouring molecules into an extended chain along the *c*-axis (Fig. 4). On the other hand, cooperative intermolecular lp(O8)···π*(C3≡O3) and π(C3≡O3)···π*(C6=C7) interactions links neighbouring molecules into an extended chain along the *b*-axis (Fig. 5).

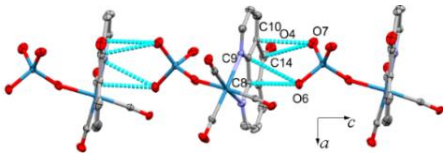

Figure 4. Representation of the intermolecular n→π* interactions involved in coordinated perrhenate.

The crystal packing of **2** was also consolidated by intermolecular C–H···O interactions (Fig. S11). A CSD search (ConQuest version 2.0.3) based on [Re(CO)$_3$(ReO$_4$)(N)(N)] query did not result in any hits but [Re(CO)$_3$(ReO$_4$)] query highlighted three structures in which [Re(CO)$_5$(ReO$_4$)] complex shows similar n→π* interactions to the title complexes.[33] To shed light on the nature of the intra- and intermolecular interactions, other suitable descriptors for bond analysis such as NBOs and non-covalent interaction index methods (NCI) were used to confirm the presence of such interactions in more detail.[34-35] Natural bond orbital calculations were performed on **1** and **2** with the same level of theory and basis sets (B3LYP/6-31G*) for non-metal atoms and LANL2DZ for Re for gas phase optimisation by Gaussian09.[36-37]

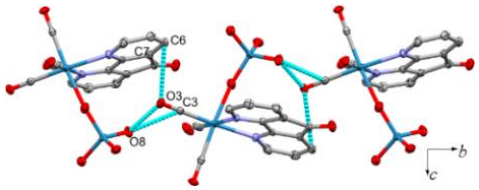

Figure 5. Representation of the intermolecular n→π* interactions involved in perrhenate and carbonyl groups in **2**.

The NBO analysis showed that the tilting of the coordinated perrhenate in **1** is due to the intramolecular n_p(O5)···π*(N2=C8) and n_p(O5)···π*(N1=C7) with overall energy of 0.22 kcal mol^{-1} while in **2** intramolecular n_s(O8)···π*(N2=C9) and n_p(O8)···π*(N2=C9) stabilize its internal geometry with total energy of 0.46 kcal mol^{-1} (Fig. 6).

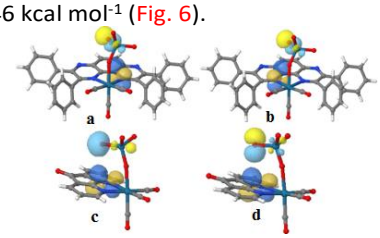

Figure 6. The intramolecular n→π* interactions (donor-acceptor orbitals) involved in perrhenate and diimine ligands in **1** (a, b) & **2** (c, d).

The donor-acceptor orbitals involved in the intramolecular π→π* interactions of the adjacent phenyl rings with the equatorial carbonyl groups influencing their bond lengths in **1**, are shown in Fig. 7. The mixing of parallel and perpendicular π(C14=C15)···π*(C2≡O2), 7a-b, and π(C26=C31)···π*(C3≡O3), 7c, account for a total energy release of 2.31 and 1.46 kcal mol^{-1} according to the NBO analysis from second-order perturbation energy, respectively (Fig. 7). The donor-acceptor orbitals involved in the interactions of **1** are based on n_s(O6)···π*(C6=C7) and n_p(O6)···π*(C6=C7) from perrhenate and n_s(O1)···π*(C6=C7) and n_s(O1)···π*(C6=C7) in carbonyl group with total energy contribution of 1.49 kcal mol^{-1}, according to the NBO analysis (Fig. 8a-d).

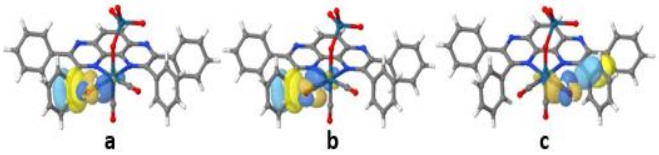

Figure 7. The donor-acceptor orbitals in π···π* interactions involved in the equatorial CO and the adjacent phenyl rings in **1**.

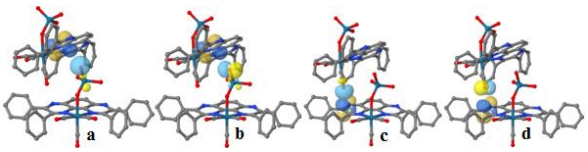

Figure 8. The donor-acceptor orbitals in n→π* interactions involved in perrhenate and carbonyl groups in **1**.

Complex **2** shows more intermolecular n→π* interactions due to the presence of carbonyl group in the skeleton of the ligand (Fig. 9e-g) and also less steric hindrance around perrhenate and carbonyl groups.

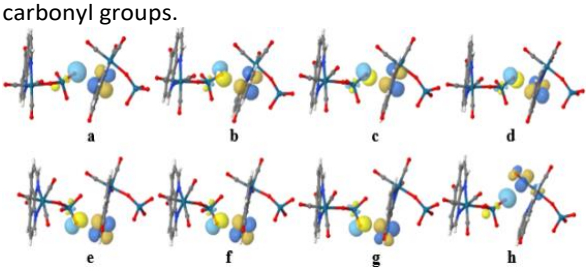

Figure 9. The donor-acceptor orbitals in n→π* interactions involved in perrhenate and carbonyl groups in **2**.

The donor-acceptor orbital interactions involved in the packing of **2** shown in Fig. 4 are based on n_s(O6)···π*(C8=N1), n_p(O6)···π*(C8=N1), n_p(O6)···π*(C8=N1), 9a-c, n_p(O6)···π*(C9=N2), 9d, n_p(O7)···π*(C10=C14), 9e, n_p(O7)···π*(C14=O4), n_p(O7)···π*(C14=O4), 9f-g, and n_p(O6)···π*(C1≡O1), 9h, with energy contribution of 0.94, 0.30, 0.38, 0.56, and 0.15 kcal mol^{-1}, respectively. In the second dimer of **2** the interacting donor-acceptor orbitals are consisting of n_s(O8)···π*(C3≡O3), n_p(O8)···π*(C3≡O3), n_p(O8)···σ*(C3≡O3), and π(C3≡O3)···π*(C6=C7) interactions with total energy contribution of 0.10, 0.24, 0.12, and 0.09, respectively (Fig. 10a-d). The last n→π* interaction in **2** is based on the mutual lp(O4)···π*(C6=C7) in the skeleton of the *Dafone* ligand forming a dimer with a total energy contribution of 0.38 kcal mol^{-1} (Fig. S12). Non-covalent interactions have also been evaluated by a complementary descriptor, the non-covalent interaction index (NCI) approach. It relies on the topological analysis of the electron density, and its derivatives at low density regions based on the reduced density gradient and also by a colour code which depicts the attractive and repulsive nature of the interactions.

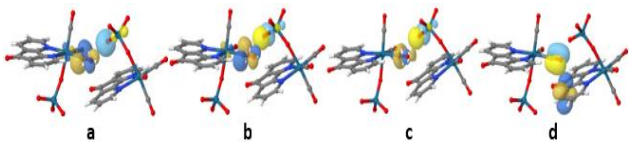

Figure 10. The n···π*, n···σ*, and π···π* donor-acceptor orbitals in perrhenate and carbonyl group interactions in **2**.

The surface NCI analysis of **1** and **2** are depicted in Fig. 11. The regions marked by black circles with blue-green colour depict

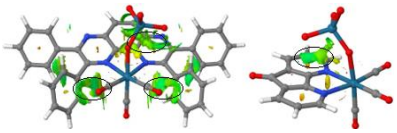

Fig. 11. NCI plots of **1** and **2** obtained directly from density cube file generated by Gaussian. The black circles show the area of intramolecular interactions in ReO_4 and CO groups.

stabilising weak intramolecular n→π* interactions related to carbonyl and perrhenate in **1** and perrhenate in **2**. Fig. 12 depicts the non-covalent interactions of the trimer of **2**. As noted, the intermolecular n→π* interactions as perpendicular lp(O1)···π*(C3≡O3), anti-parallel reciprocal C1≡O1···C1≡O1, and lp(O8)···π*(C3≡O3) with blue-green colours are marked by a, b, and c, respectively. The NCI plots of all interacting dimers mainly based on n→π* interactions in **1** and **2** are shown to agree with the region of interactions shown by X-ray and calculated by NBO method (Fig. S13-S14).

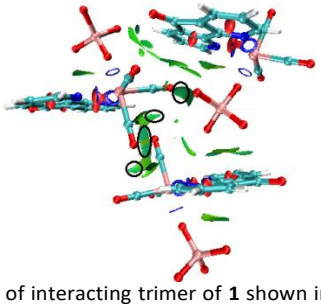

Fig. 12. NCI plot of interacting trimer of **1** shown in Fig. 3, with area of intermolecular n→π* interactions (black circles).

Conclusions

In summary, the dominant effects of the intra- and intermolecular n→π* interactions in the intramolecular geometry and supramolecular assembly of two new $Re(CO)_3$ complexes bearing diimine ligands, with a coordinated perrhenate group have been identified by X-ray crystal structure analysis, and confirmed computationally by natural bond orbitals (NBOs) and non-covalent interaction index (NCI) methods. It was shown that such interactions contribute to the molecular geometry and crystal packing of the metal carbonyl complexes and are assisted by the presence of the coordinated peroxo anion in the complexes.

Conflicts of interest

There are no conflicts to declare.

Acknowledgements

RK thanks Sharif University of Technology Research Council for Financial support. PRR is grateful to the Engineering and Physical Sciences Research Council (UK) for funding (Grant EP/K004956/1).

Notes and references

1 (*a*) J. M. Lehn, *Supramolecular Chemistry: Concepts and Perspectives*; Wiley VCH, Weinheim, 1st edn, 1995; (*b*) J. W. Steed and J. L. Atwood, *Supramolecular Chemistry*, Wiely, Chichester, 2000.
2 H. B. Bürgi, J. D. Dunitz & E. Shefter, *Nature New Bio*. 1973, **95**, 5065-5067.
3 (a) H. B. Bürgi, J. D. Dunitz, J. M. Lehn & G. Wipff, *Tetrahedron*, 1973, **30**, 1563-1572; (b) H. B. Bürgi, J. D. Dunitz & E. Shefter, *J. Am. Chem. Soc*. 1973, **95**, 5065-5067.
4 T. J. Mooibroek, P. Gamez, J. Reedijk, *CrystEngComm*, 2008, **10**, 1501-1515.
5 C. E. Jakobsche, A. Choudhary, S. J. Miller & R. T. Raines, *J. Am. Chem. Soc*., 2010, **132**, 6651-6653.
6 K. J. Kamer, A. Choudhary & R. T. Raines, *J. Org. Chem*. 2013, **78**, 2099-2103.
7 G. J. Bartlett, R. W. Newberry, B. Van Veller, R. T. Raines & D. N. Woolfson, *J. Am. Chem. Soc*., 2013, **135**, 18682-18688.
8 S. K. Singh & A. Das, *Phys. Chem. Chem. Phys*., 2015, **17**, 9596–9612.
9 R. W. Newberry & R. T. Raines, *Acc. Chem. Res*. 2017, **50**, 1838–1846.
10 S. K. Singh, K. K. Mishra, N. Sharma & A. Das, *Angew. Chem. Int. Ed*. 2016, **55**, 7801–7805.
11 G. W. Breton & C. J. Crasto, *J. Org. Chem*., 2015, **80**, 7375-7384.
12 G. W. Breton, L. O. Davis, K. L. Martin & T. A. Chambers, *Cryst. Growth Des*., 2019, **19**, 3895-3904.
13 P. Li, E. C. Vik, J. M. Maier, I. Karki, S. M. S. Strickland, J. M. Umana, M. D. Smith, P. J. Pellechia & K. D. Shimizu, *J. Am. Chem. Soc*. 2019, **141**, 12513-12517.
14 A. Rahim, P. Saha, K. K. Jha, N. Sukumar & B. K. Sarma, *Nature Commun*., 2017, **8**(78), 1-13.
15 J. C. Bristow, M. A. Addicoat, & J. D. Wallis, *CrystEngComm*, 2019, **21**, 1009-1018.
16 J. D. Velasquez, J. Echeverría & S. Alvarez, *Cryst. Growth Des*., 2019, **11**, 6511-6518.
17 B. Sahariah & B. K. Sarma, *Chem. Sci*., 2019, **10**, 909-917.
18 H. Chen, H. Ye, Y. Hai, L. Zhang & L. You, *Chem. Sci*., 2020, **11**, 2707-2715.
19 J. K. R. Deka, B. Sahariah, K. Baruah, A. K. Bar & B. K. Sarma, *Chem. Commun*., 2020, **56**, 4874-4877.
20 A. Bauza, T. J. Mooibroek & A. Frontera, *ChemPhysChem* 2015, **16**, 2496-2517.
21 (a) F. H. Allen, C. A. Baalham, J. P. M. Lommerse & P. R. Raithby, *Acta Cryst*., 1998, B**54**, 320-329; (b) H. A. Sparkes, P. R. Raithby, E. Clot, G. P. Shields, J. A. Chisholm & F. H. Allen, *CrystEngComm*, 2006, **8**, 563-570.
22 (a) J. Zukerman-Schpector, I. Haiduc & E. R. T. Tiekink, *Chem. Commun*., 2011, **47**, 12682–12684; (b) J. Zukerman-Schpector, I. Haidu & E. R. T. Tiekink, *Adv. Organomet. Chem*., 2012, **60**, 49–92.
23 C. Murcia-Garcia, A. Bauza, G. Schnakenburg, A. Frontera & R. Streubel, *CrystEngComm*, 2015, **17**, 1769-1772.
24 (*a*) J. Echeverría, *Chem. Comm*. 2018, **54** (24), 3061–3064; (*b*) J. Echeverría*, Inorg. Chem*. 2018, 57, 5429-5437.
25 (*a*) T. J. Mooibroek, *CrystEngComm*, 2017, 19, 4485-4488; (*b*) Ad r. van der Werve, Y. R. van Dijk & T. J. Mooibroek, T. J. *Chem. Commun*., 2018, **54**, 10742-10745; (c) M. T. Doppert, H. van Overeem, T. J. Mooibroek, *Chem. Commun*., 2018, **54**, 12049–12052.
26 W. F. Mark-Lee, Y. Y. Chong & M. B. Kassim, *Acta Cryst*., 2018, C**74**, 997-1006.
27 R. Kia, S. Mahmoudi & P. R. Raithby, *CrystEngComm*, 2019, **21**, 77–93.
28 R. Kia, M. Hosseini, A. Abdolrahimi & M. Mahmoudi, *CrystEngComm*, 2019, **21**, 5222-5226.
29 R. Kia & A. Kalaghchi, *Acta Cryst*., 2020, B**76**, 417-426.
30 R. Kia & A. Kalaghchi, *Crystals*, 2020, **10**(4), 267-279.

31 M. C. Chakravorti, *Coord. Chem. Rev*., 1990, **106**, 205-225.
32 A. Bondi, *J. Phys. Chem*, 1964, **68**, 441-451.
33 (*a*) C. R. Groom, I. J. Bruno, M. P. Lightfoot & S. C. Ward, *Acta Cryst*. *B*, 2016, **72**, 171-179; (*b*) G. D'Alfonso, D. Roberto, R. Ugo, C. L. Bianchi, A. Sironi, Organometallics, 2000, **19**, 2564-2572.
34 E. D. Glendening, C. R. Landis & F. Weinhold, *WIREs Comput. Mol. Sci., 2012,* **2**, 1–42.
35 E. R. Johnson, S. Keinan, P. Mori-Sánchez, J. Contreras-Garcia, A. J. Cohen, and W. Yang, *J. Am. Chem. Soc*., 2010, **132**, 6498–6506.
36 M. Frisch, *et al*., *GAUSSIAN09*. 2009. Gaussian Inc., Wallingford, CT, USA. http://www.gaussian.com.
37 P. J. Hay and W. R. Wadt, *J. Chem. Phys*., 1985, **82**, 270-83.